Original Article

Vanillic acid inhibits TGF-β type I receptor to protect bone marrow mesenchymal stem cells from radiation-induced bystander effects

Ting Zhou[1,2#], Yi-Ming Zhang[1#], Gu-Cheng Zhou[1#], Fu-Xian Liu[1], Zhi-Ming Miao[1], Li-Ying Zhang[1,3], Yang-Yang Li[1], Zhi-Wei Liu[1], Shang-Zu Zhang[1], Jing Li[1], Fan Niu[4], Yan Chen[1], Yong-Qi Liu[1,5]

[1]Provincial-Level Key Laboratory for Molecular Medicine of Major Diseases and The Prevention and Treatment with Traditional Chinese Medicine Research in Gansu Colleges and Universities, Gansu University of Chinese Medicine, Lanzhou, China; [2]Experimental & Training Teaching Centers, Gansu University of Chinese Medicine, Lanzhou, China; [3]College of Basic Medicine, Gansu University of Chinese Medicine, Lanzhou, China; [4]Affiliated Hospital of Gansu University of Chinese Medicine, Lanzhou, China; [5]Key Laboratory of Dunhuang Medicine, Ministry of Education, Lanzhou, China

Contributions: (I) Conception and design: YQ Liu; (II) Administrative support: YQ Liu; (III) Provision of study materials or patients: LY Zhang; (IV) Collection and assembly of data: T Zhou, YM Zhang, GC Zhou, ZM Miao, ZW Liu; (V) Data analysis and interpretation: FX Liu, YY Li, SZ Zhang, F Niu, J Li, Y Chen; (VI) Manuscript writing: All authors; (VII) Final approval of manuscript: All authors.

[#]These authors contributed equally to this work as co-first authors.

Correspondence to: Yong-Qi Liu, PhD. Provincial-Level Key Laboratory for Molecular Medicine of Major Diseases and The Prevention and Treatment with Traditional Chinese Medicine Research in Gansu Colleges and Universities, Gansu University of Chinese Medicine, 35 Dingxi East Road, Chengguan District, Lanzhou 730000, China; Key Laboratory of Dunhuang Medicine, Ministry of Education, Lanzhou, China. Email: lyq@gszy.edu.cn.

Background: Radiotherapy is a major treatment option for non-small cell lung cancer (NSCLC); however, irradiated tumor cells can damage non-irradiated cells through radiation-induced bystander effects (RIBE), which can affect the therapeutic efficacy. The study aimed to investigate the mechanism underlying RIBE and the protective effects of vanillic acid (VA) on human bone marrow mesenchymal stem cells (BMSCs).

Methods: We established two irradiation models to investigate RIBE. First, we established the A549 cell irradiation model alone, and tested the expression of cathepsin B (CTSB) and transforming growth factor-beta 1 (TGF-β1) by western blot and immunofluorescence staining. Next, we established a co-culture model of A549 cells and BMSCs. After 2 Gy X-rays irradiation of A549 cells, BMSCs cell viability was detected using Cell Counting Kit-8 (CCK-8), reactive oxygen species (ROS) level was detected using flow cytometry, and CTSB, TGF-β type I receptor (TGFβRI), p62 (sequestosome 1), BECLIN1, microtubule-associated protein light chain 3 (LC3), etc., were detected using western blot. Phosphorylated histone H2AX (γH2AX), CTSB, lysosomal-associated membrane protein 1 (LAMP1), and TGFβRI expression levels were detected by immunofluorescence staining. Molecular docking and molecular dynamics simulation, and a CCK-8 assay were used to screen for molecules from *Astragalus membranceus* that inhibited TGFβRI activity, to protect BMSCs from RIBE. Lastly, we validated VA activity *in vivo*.

Results: In this study, 2 Gy X-rays radiation on A549 cells was found to result in an increase in CTSB and TGF-β1, while CTSB inhibitor CA074Me reduced the radiation-induced TGF-β1 increase. In the co-culture model of A549 cells and BMSCs, 2 Gy X-rays radiation on A549 cells resulted in increase of TGFβRI expression in BMSCs, which led to an increase in ROS, and resulted in DNA damage and the inhibition of BMSCs proliferation. The small molecule VA from *Astragalus membranaceus* inhibited TGFβRI activity and restored the proliferation of BMSCs.

Conclusions: Our findings reveal that radiation causes CTSB overexpression in A549 cells, which further promotes TGF-β1 expression. TGF-β1 activates its receptors on BMSCs to increase ROS levels in BMSCs, while reducing lysosomal double-chain CTSB (dc-CTSB), which results in decreased BMSCs autophagy and an inability to clear ROS, and thus inhibits proliferation. VA inhibits TGFβRI to restore the proliferation of BMSCs, and *in vivo*, VA can enhance the killing effect of radiation on tumors.

Keywords: Bone marrow mesenchymal stem cells (BMSCs); radiation-induced bystander effects (RIBE); DNA damage; proliferation; vanillic acid (VA)

Submitted Jun 28, 2024. Accepted for publication Dec 04, 2024. Published online Feb 18, 2025.
doi: 10.21037/tcr-24-1080
View this article at: https://dx.doi.org/10.21037/tcr-24-1080

Introduction

Lung cancer is the leading cause of cancer incidence and mortality worldwide (1), and non-small cell lung cancer (NSCLC) accounts for about 85% of all incidences of lung cancer (2). Radiotherapy is a major treatment option for NSCLC (3), and irradiated cells can damage non-irradiated cells through radiation-induced bystander effects (RIBE), which can reduce the therapeutic efficacy of radiation therapy (4-6). Ionizing radiation (IR) can promote an inflammatory response, cause DNA oxidative damage, impair stem cell function (7,8), and affect therapeutic efficacy (9). Stem cells can participate in the repair of radiation-induced tissue damage (10,11). RIBE can also cause genomic instability in human bone marrow mesenchymal stem cells (BMSCs) (12), which may promote tumor progression. Transforming growth factor-beta 1 (TGF-β1) is an important factor in RIBE (13,14). A previous study found that TGF-β1 increased reactive oxygen species (ROS) production in BMSCs via binding with its receptors on BMSCs, which leads to BMSCs damage (15). Cathepsin B (CTSB) is a proteolytic enzyme that is highly expressed in many tumor tissues and is secreted into the tumor microenvironment to promote tumor progression (16-20). There are three forms of CTSB: pro-CTSB of 43 kDa in the Golgi and transport vesicles (TV), mature-CTSB of 33–36 kDa in late endosomes, and lysosomal double-chain CTSB (dc-CTSB) of 24–25 kDa in lysosomes (21), which mainly participate in the regulation of autophagy (22). CTSB can cause RIBE in *Caenorhabditis elegans* (*C. elegans*) (23), and TGF-β1 can upregulate CTSB expression in tumor cells (24). CTSB can also promote the autocrine function of TGF-β1 (25). In this study, we preliminarily investigated the relationship of CTSB and TGF-β1 in irradiated A549 cells, and the relationship between TGF-β type I receptor (TGFβRI) activation and dc-CTSB in bystander BMSCs.

Vanillic acid (VA) is a compound widely found in Chinese herbal medicines, including *Astragalus membranaceus*, which can regulate different cytokines to inhibit inflammation and the immune response (26). In this study, we investigated the protective effects of VA on BMSCs in a co-culture irradiation model. The results showed that VA could decrease the RIBE in BMSCs via inhibiting the activity of TGFβRI. VA may have potential as an adjuvant drug to reduce the RIBE in patients with lung cancer who receive radiotherapy. We present this article in accordance with the ARRIVE reporting checklist (available at https://tcr.amegroups.com/article/view/10.21037/tcr-24-1080/rc).

Highlight box

Key findings

- This study discovered that vanillic acid (VA) can reduce the bystander effects of irradiated lung cancer cells on human bone marrow mesenchymal stem cells (BMSCs) by inhibiting transforming growth factor-beta type I receptor (TGFβRI).

What is known and what is new?

- Irradiated lung cancer cells can damage non-irradiated bystander BMSCs through radiation-induced bystander effects (RIBE), and transforming growth factor-beta 1 (TGF-β1) is an important bystander factor.
- TGF-β1 binds to its receptors on BMSCs, leading to an increase of lysosomal cathepsin B and an increase in reactive oxygen species, resulting in DNA damage and inhibition of BMSCs proliferation. VA can inhibit the activity of TGFβRI and reduce the RIBE of lung cancer cells on BMSCs.

What is the implication, and what should change now?

- Targeting TGFβRI on BMSCs may provide a viable therapeutic modality for reducing RIBE and improving the efficacy of radiotherapies.

Methods

Cell culture

Human lung adenocarcinoma A549 and H1299 cells, human bronchial epithelial cells BEAS-2B (B2B), and mouse lung cancer Lewis cells were purchased from Shanghai Institute for Biological Sciences (Shanghai, China). A549 were cultured in Dulbecco's modified Eagle's medium (DMEM)/nutrient mixture F-12 medium (1:1, DMEM/F-12) with

10% fetal bovine serum (Clark, Richmond, VA, USA) and 100 μg/mL penicillin and streptomycin in a 5% CO_2 humidified incubator at 37 ℃. H1299, B2B, and Lewis cells were cultured in DMEM with 10% fetal bovine serum (Clark) and 100 μg/mL penicillin and streptomycin in a 5% CO_2 humidified incubator at 37 ℃. Human BMSCs (ScienCell, San Diego, CA, USA) were maintained in mesenchymal stem cell medium (MSCM) (7501, ScienCell) special medium at 37 ℃ in 5% CO_2.

Antibodies and agents

Anti-TGFβRI antibody, anti-p62 antibody, anti-BECLIN1 antibody, and anti-microtubule-associated protein light chain 3 (LC3) antibody were obtained from Abcam (Cambrige, UK). Anti-histone phosphorylated histone H2AX (γH2AX) antibody and anti-lysosomal-associated membrane protein 1 (LAMP1) antibody were purchased from GeneTex (Irvine, CA, USA). Anti-CTSB antibody, anti-glyceraldehyde 3-phosphate dehydrogenase (GAPDH) antibody, anti-β-actin antibody, goat-anti rabbit horseradish peroxidase (HRP)-conjugated secondary antibody, goat-anti mouse HRP-conjugated secondary antibody, goat-anti rabbit 594, and goat-anti mouse 488 were purchased from Immunoway (Plano, TX, USA). CA074Me and SB431542 were purchased from MedChemExpress (Monmouth Junction, NJ, USA). VA was purchased from Shanghai Yuanye Bio-Technology Co., Ltd. (Shanghai, China).

Co-culture and irradiation

We established two irradiation models, one was the A549 cell irradiation model alone, and the other was the transwell co-culture model of A549 cells and BMSCs. In the co-culture model, A549 cells were seeded at 3.4×10^4 cells per well in the upper compartment and BMSCs were seeded at 1.2×10^5 cells per well in the lower compartment. A549 cells were exposed to a single dose of 2 Gy X-rays from X-RAD-225 X-rays source (Precision, North Branford, CT, USA) at a dose rate of 2 Gy/min (225.0 kV, 13.3 mA).

Groups

BMSCs were divided into five groups. BMSCs were used as controls (Ctrl group) and co-cultured with A549 cells, to serve as the co-culture group (Co group). BMSCs were also co-cultured with irradiated A549 cells (Co+IR group), and the Co+IR group was cultured with 20 μmol/L TGFβRI inhibitor SB431542 (Co+IR+SB group), or with 25 μmol/L VA (Co+IR+VA group).

Cell proliferation assay

Cell morphology was observed by a microscope (OLYMPUS, Tokyo, Japan). Cell proliferation was tested using a Cell Counting Kit-8 (CCK-8) test kit (Dojindo, Kumamoto, Japan), according to the manufacturer's instructions. The BMSCs were seeded in 96-well plates at a density of 4×10^3 cells/well. A549, H1299, and B2B cells were seeded into 96-well plates at a density of 2×10^3 cells per/well. The absorbance values were read at 450 nm using a microplate reader.

Western blot analysis

The cells were lysed in radioimmune precipitation assay (RIPA) buffer for 10 min. Proteins were resolved using 10% sodium dodecyl sulfate-polyacrylamide gel electrophoresis (SDS-PAGE) and transferred onto methanol-activated polyvinylidene fluoride (PVDF) membranes for western blotting.

Immunofluorescence staining

The cells were cultured on coverslips, harvested 48 h after irradiation, fixed in 4% polyformaldehyde for 15 min, and permeabilized in PBS containing 0.5% Triton-X 100 for 5 min. The samples were blocked with 5% goat serum for 2 h and then incubated with γH2AX, CTSB, LAMP1, and TGFβRI antibody for 2 h at room temperature, followed by incubation with secondary antibody for 2 h at room temperature, counterstaining with 4',6-diamidino-2-phenylindole (DAPI) for 10 min, and visualization using a confocal microscope.

Flow cytometric analysis of ROS levels

ROS levels in BMSCs were detected by flow cytometry, according to the manufacturer's instructions.

Animals

We conducted experiments using SPF-grade male C57BL/6 mice aged 6–8 weeks and weighing 18–22 g. Animals were randomly divided into four groups: control group (Ctrl), tumor group (Tumor), tumor with 4 Gy X-rays

irradiation group (Tumor+IR), and tumor + IR group with oral administration of 30 mg/kg VA (Tumor+IR+VA), with six animals in each group (a total of 24 animals). The animals were provided by the Lanzhou Veterinary Research Institute, Chinese Academy of Agricultural Sciences, under the license number SCXK (Gan) 2020-002. A protocol was prepared before the study without registration. All experiments were approved by the Ethics Committee of Gansu University of Chinese Medicine (Number of Animal Experimental Ethical Inspections of Gansu University of Chinese Medicine: 2019-153), in compliance with Gansu University of Chinese Medicine guidelines for the care and use of animals. All animals were housed in a controlled room (temperature, 25±2 ℃; relative humidity, 45–60%; lighting cycle, 12 h/d; 06:30–18:30 for light) with sufficient food and water supply.

Subcutaneous lung cancer tumor model

The animals were subcutaneously inoculated with 0.2 mL of a 1×10^7 cells/mL Lewis cells suspension into the right forelimb. Animal health, behavior, and tumor size were monitored daily. On the 7th day, when the tumors had grown to 3–6 mm, the mice were anesthetized with 0.3% pentobarbital sodium at a dose of 0.1 mL/10 g. The head and other parts of the mouse body were then covered with a lead plate to expose only the tumor tissues. Tumor tissues were irradiated with 4 Gy X-rays. Based on the dose reported in the literature (27,28), 30 mg/kg of VA was immediately injected into the abdominal cavity. After continuous administration for 7 days, the animals were sacrificed on the 7th day after irradiation to obtain samples for subsequent experiments.

Statistical analysis

The data were analyzed with SPSS 26.0 statistical software. The statistical significance of the data between different groups was calculated using one-way analysis of variance (ANOVA) or Student's *t*-test. P<0.05 was considered statistically significant.

Results

Radiation-induced high CTSB expression in A549 cells promotes TGF-β1 expression

We first detected CTSB and TGF-β1 in A459 cells after exposure to 2 Gy X-rays radiation. The results showed that, compared with the Ctrl group, the expression of mature-CTSB (P<0.01) and TGF-β1 (P<0.05) increased at 12, 24, and 48 h after irradiation (*Figure 1A-1D*). Next, to investigate whether the high expression of CTSB after radiation further elevated TGF-β1 expression, CTSB inhibitor CA074Me (10 μM) was added to the culture medium, which reduced radiation-induced TGF-β1 expression (P<0.01) (*Figure 1E,1F*). Interestingly, we further detected the co-localization of CTSB and the lysosomal membrane protein LAMP1 through immunofluorescence staining, and found that the localization of CTSB changed after irradiation (*Figure 1G-1J*). Compared to the control group, CTSB expression in lysosomes decreased after irradiation (P<0.01), whereas CTSB expression around the cell membrane increased.

Increased ROS caused by A549 irradiation decreased BMSCs autophagy and restored proliferation

First, we evaluated BMSCs proliferation after co-culturing with irradiated A549 cells for 48 h. Cell proliferation was decreased in the Co group (P<0.05) and Co+IR group (P<0.01) (*Figure 2A,2B*), and the ROS levels in the BMSCs of the Co and Co+IR groups also increased after 48 h (P<0.01) (*Figure 2C,2D*). To investigate whether ROS caused DNA damage in BMSCs, we investigated the expression of γH2AX by immunofluorescence staining (*Figure 2E*). Compared with the Ctrl group, the γH2AX foci number increased in the BMSCs of the Co and Co+IR groups.

To investigate whether the accumulation of ROS was caused by decreased autophagy, the expression of autophagy-related proteins was detected in BMSCs. Compared with the Ctrl group, the expression of BECLIN1 and p62 proteins was reduced in the Co group (P<0.01), while there was no statistically significant difference in the expression of LC3-II (P>0.05) (*Figure 2F-2I*). Compared to the Co group, the expression of BECLIN1, p62, and LC3-II was also reduced in the Co+IR group (P<0.05) (*Figure 2F-2I*). In addition, owing to the close relationship between CTSB and autophagy, we also detected CTSB expression in BMSCs. We found that dc-CTSB expression was higher in the Co+IR group than in the Ctrl and Co groups, respectively (P<0.01) (*Figure 2E,2J*).

TGF-β1 pathway activation promotes an increase in dc-CTSB in BMSCs

As mentioned earlier, the expression of TGF-β1 in A549

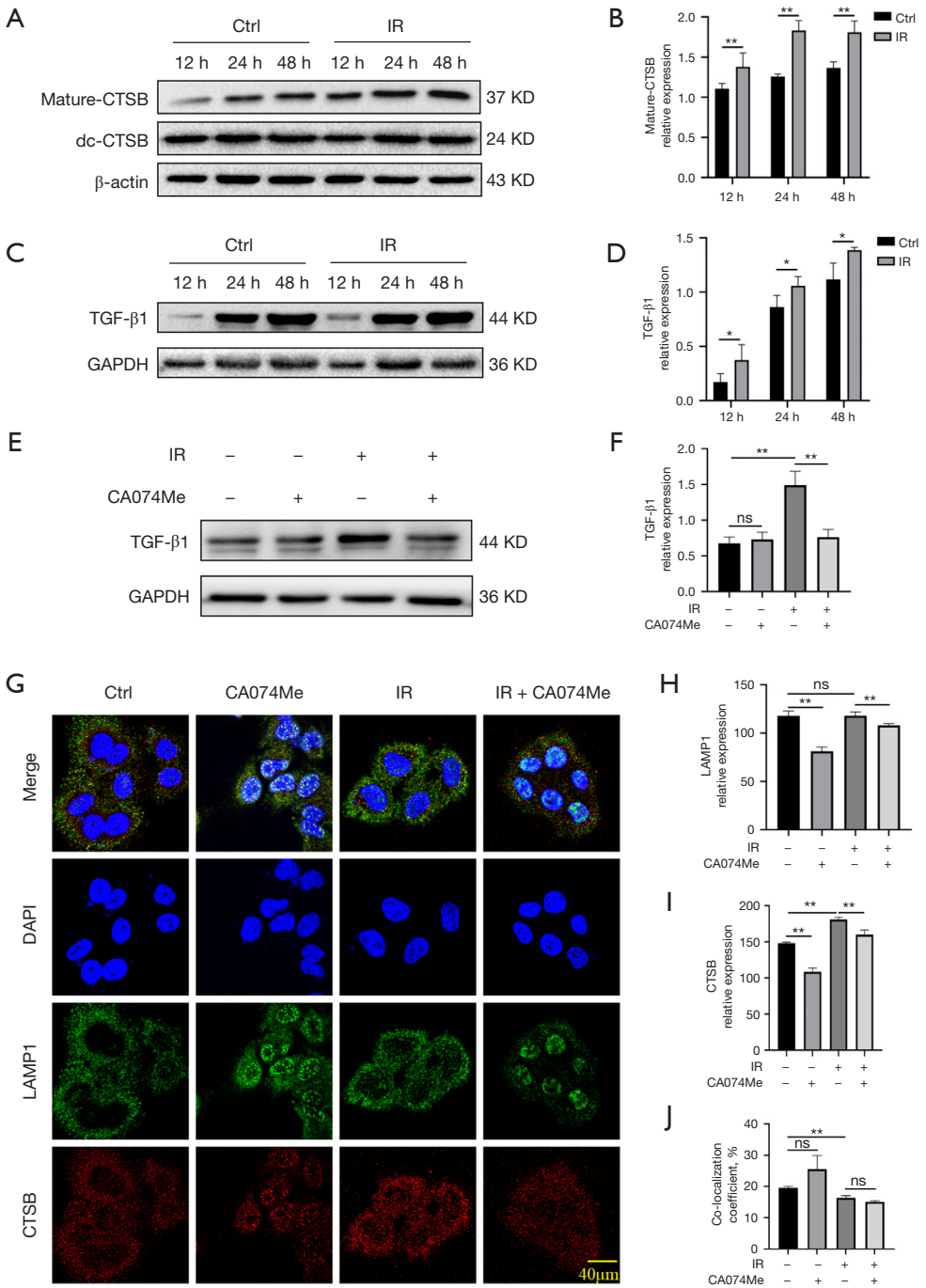

Figure 1 Radiation-induced upregulation of CTSB and TGF-β1 in A549 cells. (A) Western blotting of mature-CTSB and dc-CTSB. (B) Statistical protein results of mature-CTSB. (C) Western blot bands of TGF-β1. (D) Protein statistical results of TGF-β1. (E) Western blot bands of TGF-β1 in A549 cells after treatment with 10 μM CA074Me. (F) Protein statistical results of TGF-β1. (G) Immunofluorescence detection of LAMP1 and CTSB by confocal microscope (600× magnification). (H) Statistical analysis of LAMP1 expression. (I) Statistical results of the CTSB protein analysis. (J) Statistical results of the co-localization coefficient of LAMP1 and CTSB. *, P<0.05; **, P<0.01; ns, no significance. Ctrl, controls; IR, ionizing radiation; CTSB, cathepsin B; dc-CTSB, lysosomal double-chain CTSB; TGF-β1, transforming growth factor-beta 1; GAPDH, glyceraldehyde 3-phosphate dehydrogenase; CA074Me, CA074 methyl ester, CTSB inhibitor; DAPI, 4',6-diamidino-2-phenylindole; LAMP1, lysosomal-associated membrane protein 1.

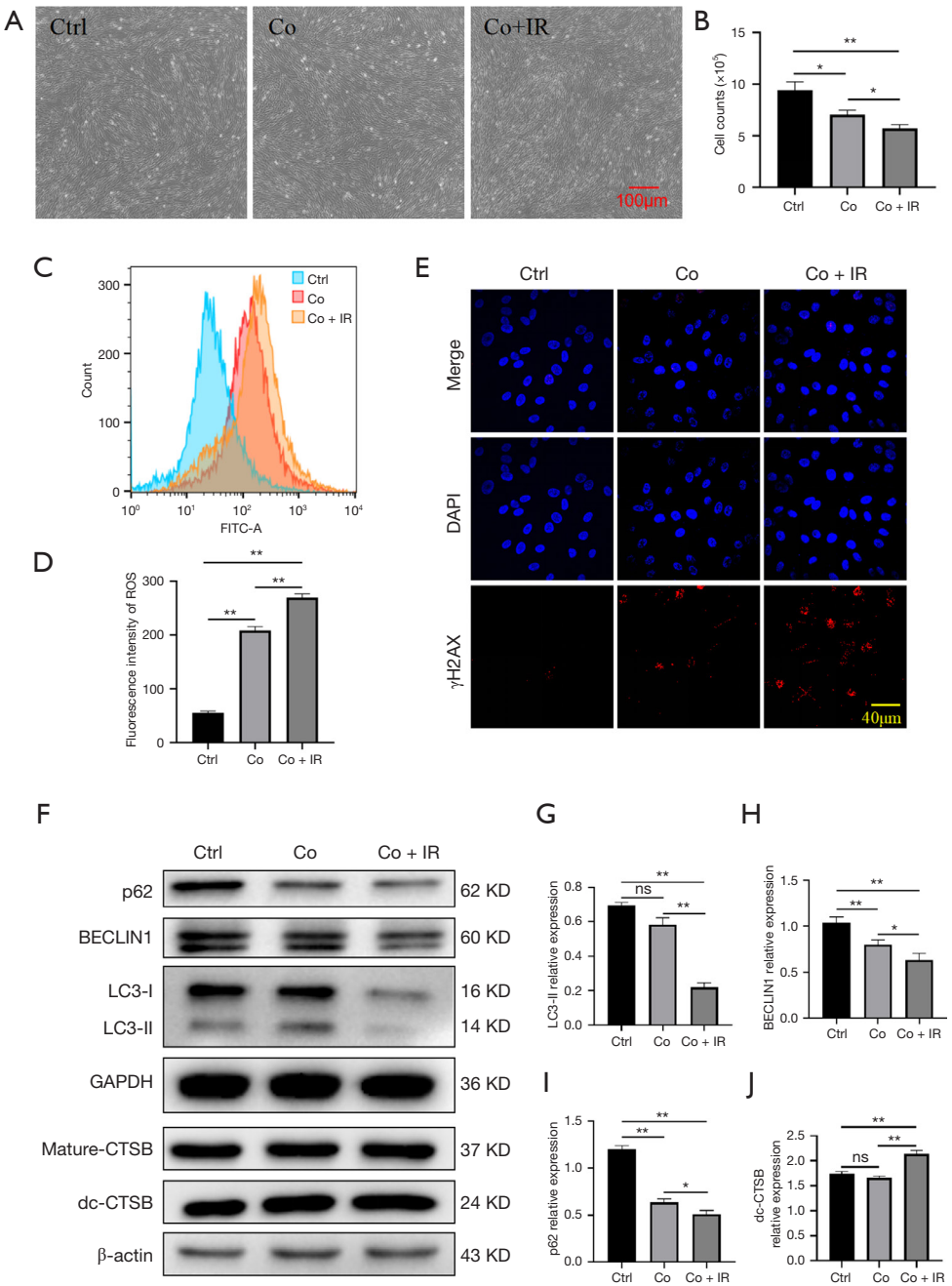

Figure 2 DNA damage and autophagy inhibition in BMSCs after A549 irradiation. (A) Morphology of BMSCs (40× magnification) was observed and photographed by a microscope. (B) Cell counts. (C) Relative ROS levels in BMSCs obtained by flow cytometry. (D) Statistical analysis of ROS levels. (E) Immunofluorescence images of γH2AX that were taken using a confocal microscope (600× magnification). (F) Western blotting bands for p62, BECLIN1, LC3-I, LC3-II, mature-CTSB, and dc-CTSB. (G) The protein statistical results for LC3-II. (H) Statistical analysis of BECLIN1 expression. (I) Statistical analysis of p62. (J) The protein statistical result of dc-CTSB. *, P<0.05; **, P<0.01; ns, no significance. Ctrl, controls; Co, co-culture; IR, ionizing radiation; ROS, reactive oxygen species; FITC, fluorescein isothiocyanate; DAPI, 4',6-diamidino-2-phenylindole; γH2AX, phosphorylated histone H2AX; p62, sequestosome 1; LC3-I, microtubule-associated protein light chain 3 type I; LC3-II, microtubule-associated protein light chain 3 type II; CTSB, cathepsin B; dc-CTSB, lysosomal double-chain CTSB; BMSCs, bone marrow mesenchymal stem cells.

increases after irradiation. Our prior study showed that the TGF-β1 concentration in co-culture medium increases after irradiation (29). To verify if the high level of TGF-β1 in the medium activated the TGF-β pathway in BMSCs, we evaluated TGFβRI expression using immunofluorescence staining (*Figure 3A*). Notably, TGFβRI was overexpressed in the Co group (P<0.05) and Co+IR group (P<0.01), compared with the Ctrl group (*Figure 3B*). In addition, TGFβRI increased after irradiation, compared with the Co group (P<0.05). A prior study has reported that TGF-β1 can promote CTSB expression in tumor cells (24). Therefore, the TGFβRI inhibitor SB431542 (20 μM) was added to the culture medium, and western blot and immunofluorescence staining were performed to evaluate dc-CTSB expression in lysosomes (*Figure 3C-3H*). The results showed that SB431542 significantly decreased dc-CTSB expression (P<0.05) (*Figure 3C,3D*). In addition, the expression of CTSB, LAMP1, and co-localization of CTSB and LAMP1 significantly decreased in the presence of SB431542 (P<0.01) (*Figure 3E-3H*). These results indicate that the inhibition of TGFβRI in BMSCs can suppress dc-CTSB expression.

Screening of functional compounds from Astragalus membranaceus to inhibit TGFβRI in BMSCs

In this study, VA was screened from a compound library of *Astragalus membranaceus* molecules that were tested for influencing the viability of BMSCs (*Figure 4A*), B2B (*Figure 4B*), A549 (*Figure 4C*), and H1299 (*Figure 4D*) cells using the CCK-8 assay. We screened the safe drug concentration of VA (*Figure 4A,4B*). The results suggest that 6.25–25 μM VA promotes the proliferation of BMSCs and B2B cells. Furthermore, the results suggest that VA at 25–100 μM inhibits the A549 cell proliferation (*Figure 4C*), and VA at 50–100 μM inhibits the H1299 cell proliferation (*Figure 4D*). In summary, 25 μM VA was selected as the intervention concentration in this study. Molecular docking and molecular dynamics simulations were used to verify the binding activity of VA and TGFβRI (*Figure 4E-4H*). The results showed that VA could interact with Lys232 and Lys337 to form a salt bridge, and form hydrogen bonds with Asp351 and Ser280 and hydrophobic interactions with Lys232, Leu260, and Leu340 (*Figure 4E*). The binding free energy between TGFβRI and VA was –18.22±3.33 kcal/mol, which suggests a high-affinity interaction. The root mean square deviations (RMSD) of molecular dynamics simulation was maintained at about 2Å, which indicates that the TGFβRI protein is stable in combination with VA (*Figure 4F*). Simultaneously, VA and TGFβRI can form an additional two hydrogen bonds during the molecular dynamics simulation process (*Figure 4G*). The root mean square fluctuation (RMSF) of the TGFβRI and VA complex was about 2Å, indicating that VA may improve TGFβRI protein stability (*Figure 4H*). The above results suggest that VA inhibits TGFβRI activation by direct binding.

VA decreased bystander effects by targeting TGFβRI in BMSCs in vitro and repressed tumor growth in vivo

We further tested the activity of VA towards TGFβRI *in vitro* and found that 25 μmol/L VA significantly increased BMSCs proliferation (P<0.01) (*Figure 5A,5B*). In addition, TGFβRI expression was downregulated in the Co+IR+VA group compared with the Co+IR group (P<0.01) at the mRNA and protein levels, respectively (*Figure 5C-5E*). To verify whether VA can enhance the killing effect of radiation on tumors, we compared the effects of simple irradiation and irradiation with VA (25 μmol/L) on A549 cell viability (*Figure 5F*). The results showed that VA significantly reduced the A549 cell viability. Interestingly, we also found that VA combined with IR reduced the tumor size and weight (P=0.16) (*Figure 5G-5I*). These results show that VA can not only reduce RIBE via inhibiting TGFβRI, but also enhance the killing effect of radiation on tumors. A previous study by Sutthibhon *et al.* showed that VA restored cell viability after UVB exposure by reducing intracellular ROS and nitric oxide (NO), lowering downstream mitogen-activated protein kinase (MAPK) pro-inflammatory cascade reactions, and can be used in the research of antioxidants and anti-inflammatory drugs (30). Another study by Wu *et al.* indicated that VA can inhibit triple-negative breast cancer (TNBC) cell proliferation, migration, and invasion through Janus kinase (JAK)/signal transducer and activator of transcription 3 (STAT3) signaling (31). These above research results are similar to our findings. Although there was no statistical difference between the IR+VA and IR groups *in vivo*, the tumor size and volume showed a decreasing trend. We will further explore the role of VA in future work.

Discussion

Radiation-induced ROS strongly promotes the activation of NOD-like receptor family pyrin domain containing 3 (NLRP3) inflammatory bodies (32), as well as the overexpression of TGF-β1, tumor necrosis factor-alpha

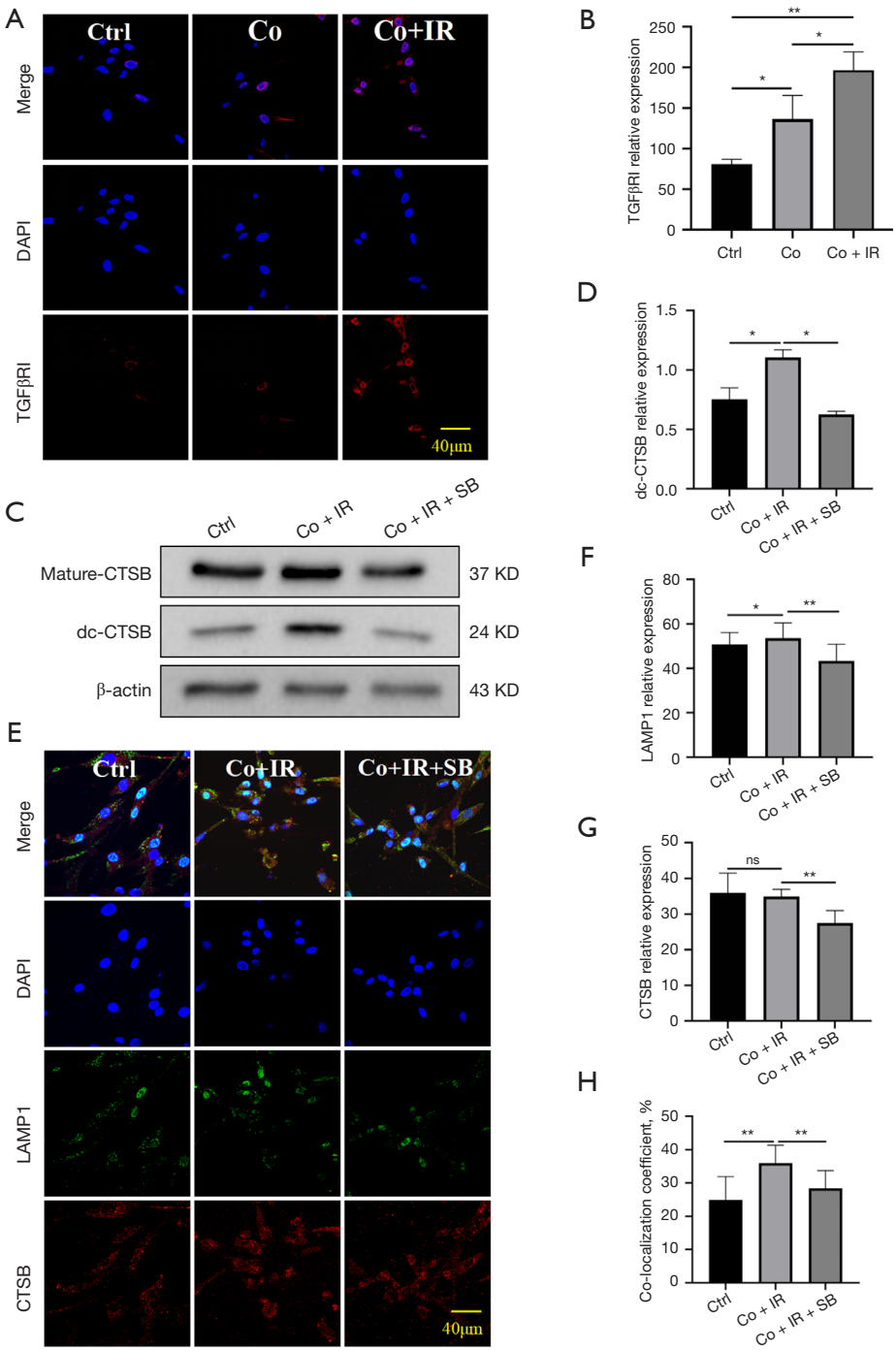

Figure 3 TGFβRI activation stimulates expression of dc-CTSB in BMSCs after irradiation. (A) The immunofluorescence images of TGFβRI by confocal microscopy (600× magnification). (B) Protein statistical analysis results of TGFβRI. (C) Western blot bands of mature-CTSB and dc-CTSB in A549 cells after treatment with 20 μM SB431542. (D) Statistical analysis of dc-CTSB protein expression. (E) Immunofluorescence images of LAMP1 and CTSB that were obtained using a confocal microscope (600× magnification). (F) Statistical analysis of LAMP1 expression. (G) Statistical analysis of CTSB protein expression. (H) Statistical results of the co-localization coefficient of LAMP1and CTSB. *, P<0.05; **, P<0.01; ns, no significance. Ctrl, controls; Co, co-culture; IR, ionizing radiation; DAPI, 4',6-diamidino-2-phenylindole; TGFβRI, transforming growth factor-beta type I receptor; SB, SB431542; dc-CTSB, lysosomal double-chain CTSB; CTSB, cathepsin B; LAMP1, lysosomal-associated membrane protein 1.

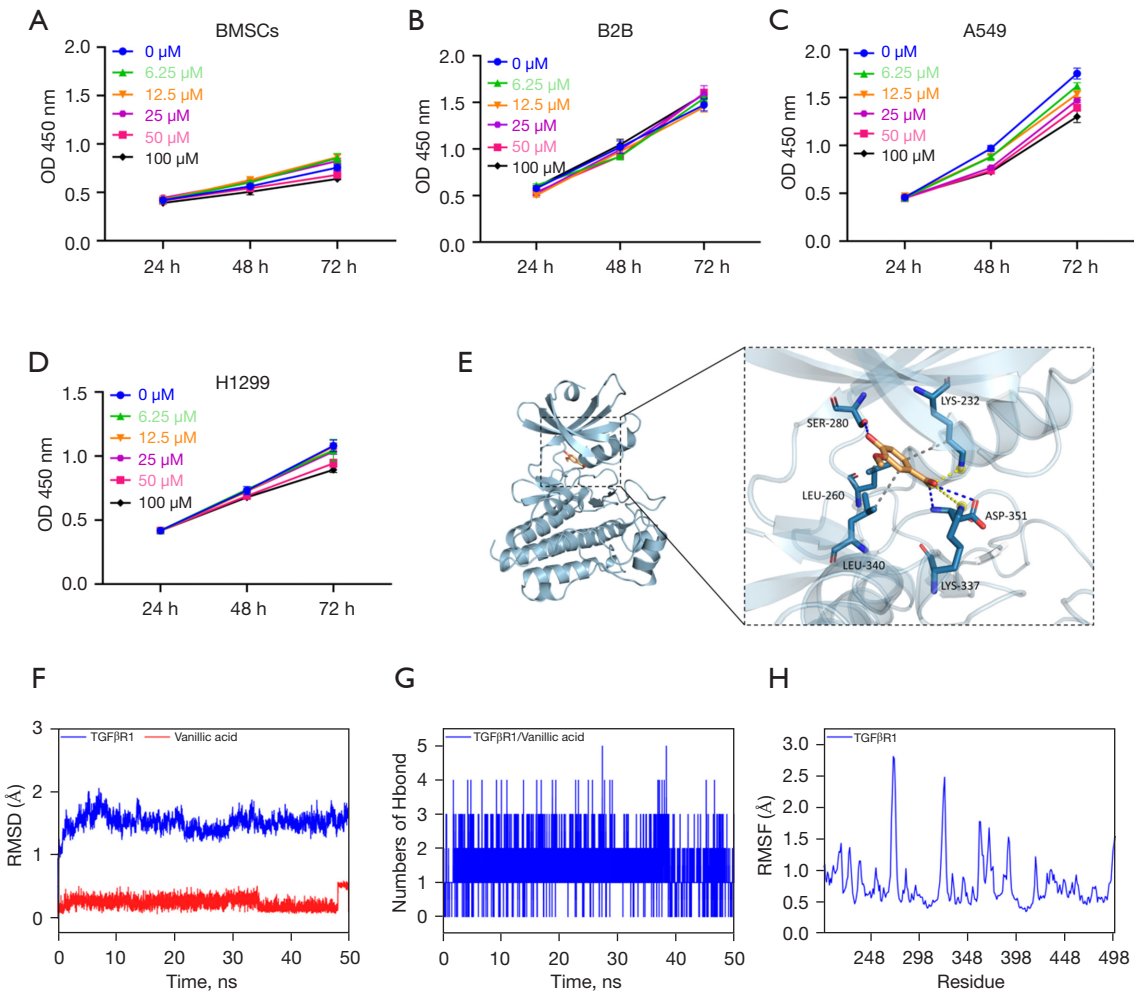

Figure 4 Screening of VA from Astragalus as an inhibitor of TGFβRI. (A-D) Proliferation of BMSCs and B2B, A549, and H1299 cells, as detected using the CCK-8 assay. (E) Crystal structure and amino acid sites of TGFβRI. (F) The RMSD value of TGFβRI and VA. (G) The hydrogen bonds formed between TGFβRI and VA. (H) The RMSF value of TGFβRI and VA. OD, optical density; BMSCs, bone marrow mesenchymal stem cells; RMSD, root mean square deviations; RMSF, root mean square fluctuation; TGFβRI, transforming growth factor-beta type I receptor; VA, vanillic acid; CCK-8, Cell Counting Kit-8.

(TNF-α), interleukin-6 (IL-6), etc. (6,33-36). In the present study, we found that irradiated A549 cells highly expressed mature-CTSB and TGF-β1, and the inhibition of CTSB reduced the IR-induced high TGF-β1 expression. Further, we found that activated TGFβRI and dc-CTSB overexpression in BMSCs, leads to DNA damage and inhibits proliferation. We further discovered that the inhibition of TGFβRI decreased dc-CTSB expression, which builds upon the findings of Yang *et al.* (37), who discovered that the activation of TGFβRI induced SMAD family member 3 (SMAD3) translocating into nucleus inhibited transcription factor EB (TFEB) expression, suppressed lysosomes biogenesis, and prevented damaged lysosome clearance, which led to lysosome depletion in tubular epithelial cells. Furthermore, the inhibition of SMAD3 reduced the accumulation of damaged lysosomes and expression of dispersed CTSB in a model of diabetic nephropathy (37). Autophagy can encapsulate old and damaged lipids, proteins, and organelles in autophagosomes and transport them to lysosomes for recycling (38), while clearing excess ROS to protect cells from oxidative damage (39). Autophagy also prevents radiation damage by reducing ROS production in stem cells (40). The lack of CTSB in bone marrow-derived macrophages (BMDMs)

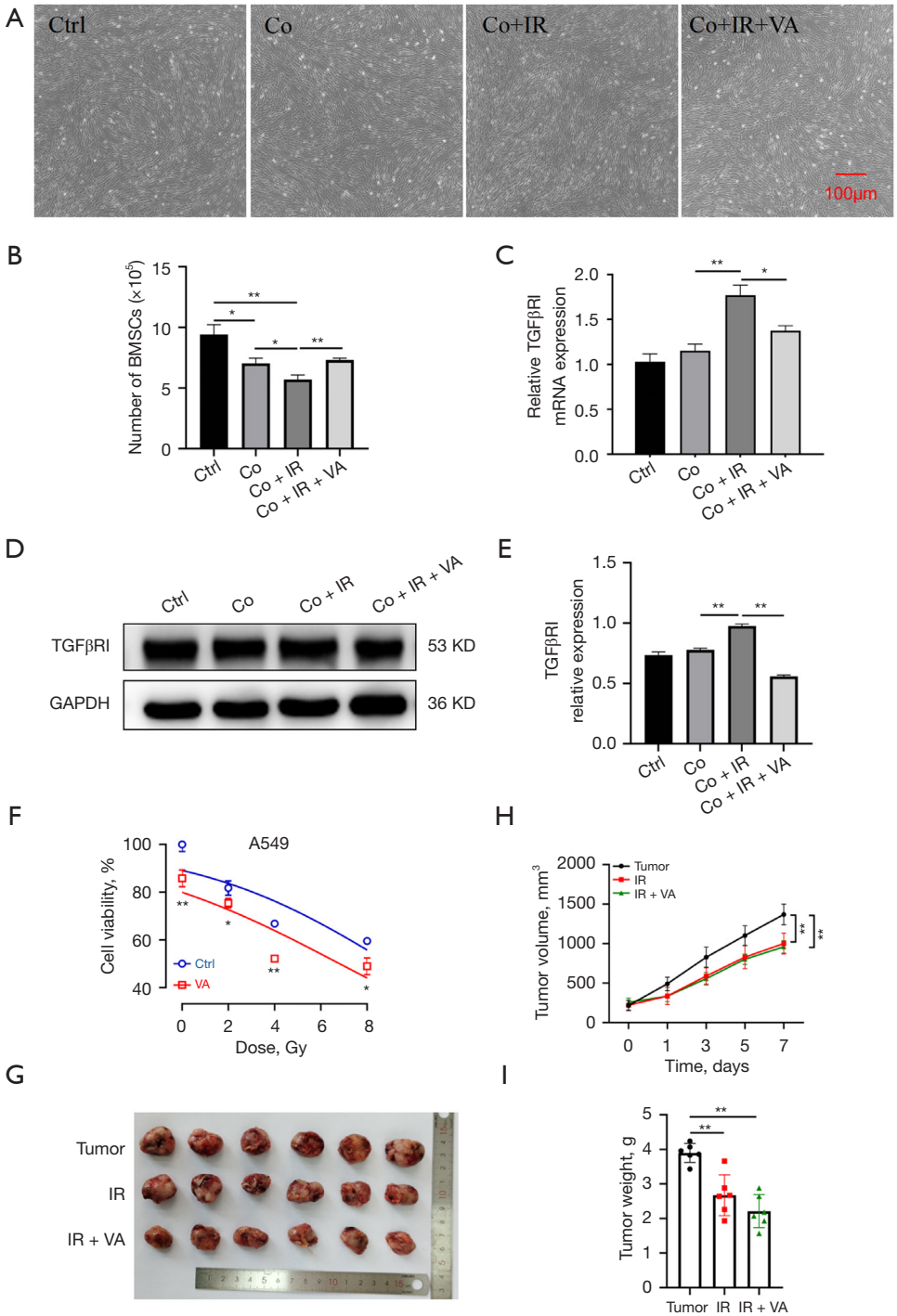

Figure 5 VA reduced bystander effects of BMSCs after irradiation of A549 cells. (A) Morphology of co-cultured BMSCs treated with VA for 48 h after irradiation (40× magnification), cells were imaged by a microscope. (B) Cell count. (C) TGFβRI mRNA expression. (D) Western blot bands of TGFβRI. (E) Protein statistical results of TGFβRI. (F) The effect of VA combined with radiation on the cell viability of A549 cells under single radiation with different radiation doses (n=3). (G) Morphology of tumor tissues (n=6) in C57BL/6 mice with or without VA treatment. (H,I) Tumor volume and weight in each group. *, P<0.05; **, P<0.01. Ctrl, controls; Co, co-culture; IR, ionizing radiation; VA, vanillic acid; BMSCs, bone marrow mesenchymal stem cells; TGFβRI, transforming growth factor-beta type I receptor; GAPDH, glyceraldehyde 3-phosphate dehydrogenase.

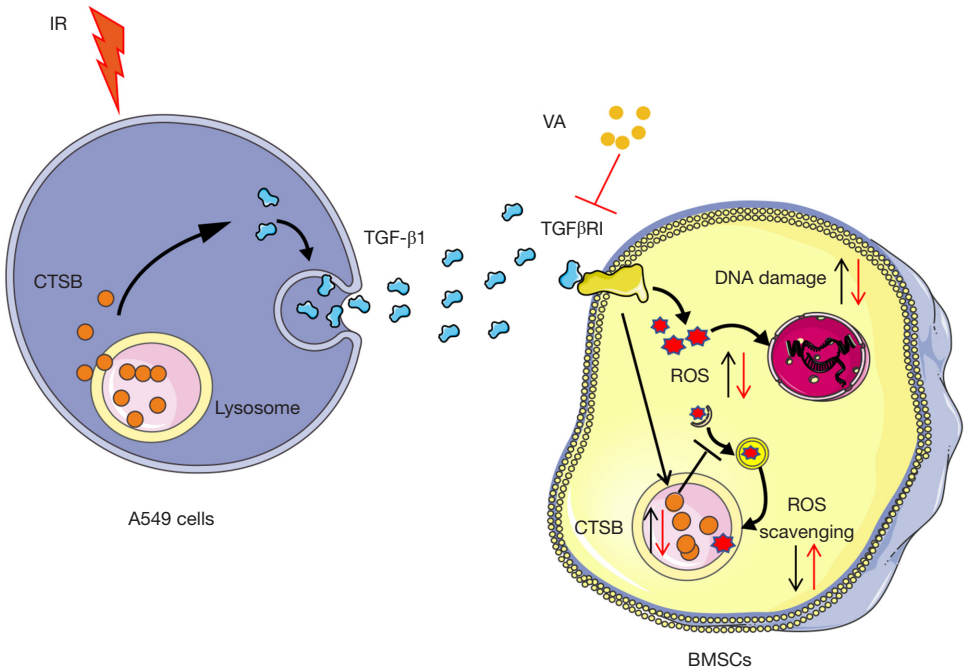

Figure 6 The mechanism of the protective effect of VA in BMSCs. In summary, TGF-β1 produced by irradiated A549 cells activated TGFβRI on bystander BMSCs. Activated TGFβRI, on one hand, can increase the production of ROS, and on the other hand, can inhibit the degradation of ROS by promoting the expression of dc-CTSB, which ultimately inhibits BMSCs proliferation. Furthermore, VA can protect BMSCs from RIBE by inhibiting TGFβRI activity. The black arrows represent the changes in intracellular proteins and ROS in A549 cells and BMSCs after radiation, while the red arrows represent the changes in intracellular proteins and ROS after VA treatment. IR, ionizing radiation; CTSB, cathepsin B; TGF-β1, transforming growth factor-beta 1; VA, vanillic acid; TGFβRI, transforming growth factor-beta type I receptor; ROS, reactive oxygen species; BMSCs, bone marrow mesenchymal stem cells; dc-CTSB, lysosomal double-chain CTSB; RIBE, radiation-induced bystander effects.

increases the number and size of single-membrane lysosomes and double-membrane autophagosomes (22).

This research supports our hypothesis that TGF-β1 overexpression and secretion after the irradiation of A549 cells activates TGFβRI on BMSCs. This, on the one hand, leads to an increase in ROS production in BMSCs, and, on the other hand, upregulates lysosomal dc-CTSB and inhibits autophagy. Therefore, the ROS produced by oxidative stress cannot be cleared efficiently, which affects BMSCs proliferation and genomic stability. One of our previous studies has shown that Astragalus polysaccharide (APS) can inhibit ROS-induced mitochondrial apoptosis induced by ROS from irradiated A549 cells (41). Selective pharmacological inhibition of CTSB significantly upregulated the mRNA and protein levels of selective autophagy substrate p62 and LC3-II in human skin fibroblasts (42). Notably, Zheng *et al.* previously illustrated that the inhibition of CTSB blocks RIBE in *C. elegans* (43).

VA showed anti-inflammatory effects in Huntington's disease by targeting the IKK-NF-κB pathway (44). VA also attenuates H_2O_2-induced injury in H9C2 cells by modulating mitophagy via the PINK1/Parkin/Mfn2 pathway, which improves impaired autophagic flux, increases the ratio of LC3-II/LC3-I, and reduces p62 expression (45). Using molecular docking and dynamic simulation, we determined that the combination of VA and TGFβRI is the best and most stable, and 25 μmol/L VA showed significant inhibition activity to TGFβRI to reduce the RIBE on BMSCs.

In conclusion, irradiated A549 cells overexpress CTSB and TGF-β1, which CTSB can further increase TGF-β1. TGF-β1 interacts with its receptor on BMSCs, on the one hand, to produce more ROS, and on the other hand, to promote the expression of TGFβRI to reduce the RIBE in BMSCs. This, it would be appropriate to further explore the potential of VA to be used as an adjuvant drug for lung cancer radiotherapy (*Figure 6*).

In summary, this study provides a reference for

protection against bystander effects caused by radiotherapy in lung cancer. However, it remains unclear why tumor-associated BMSCs overexpress CTSB. However, the specific mechanism by which CTSB regulates the increase in TGF-β1 expression still needs further exploration. In addition, our study involved only the bystander effect models of one-time irradiation. Whether the same mechanism leads to long-term repeated radiation therapy should be investigated in future studies.

Conclusions

Radiation causes CTSB overexpression in A549 cells to further promote TGF-β1 expression. TGF-β1 activates its receptors on BMSCs to cause an increase in ROS in BMSCs, while reducing lysosomal dc-CTSB, which results in decreased BMSCs autophagy, and inability to clear ROS, and proliferation inhibition. VA can inhibit the activity of TGFβRI to restore the proliferation of BMSCs, and *in vivo*, VA can enhance the killing effect of radiation on tumors.

Acknowledgments

We acknowledge Gansu University of Chinese Medicine, Provincial-Level Key Laboratory for Molecular Medicine of Major Diseases and The Prevention and Treatment with Traditional Chinese Medicine Research in Gansu Colleges and Universities, and Key Laboratory of Dunhuang Medicine, Ministry of Education for their support of this research.

Footnote

Reporting Checklist: The authors have completed the ARRIVE reporting checklist. Available at https://tcr.amegroups.com/article/view/10.21037/tcr-24-1080/rc

Data Sharing Statement: Available at https://tcr.amegroups.com/article/view/10.21037/tcr-24-1080/dss

Peer Review File: Available at https://tcr.amegroups.com/article/view/10.21037/tcr-24-1080/prf

Funding: This study was supported by the National Natural Science Foundation of China (No. 81973595) and the Provincial Natural Science Foundation of Gansu (No. 22JR11RA115).

Conflicts of Interest: All authors have completed the ICMJE uniform disclosure form (available at https://tcr.amegroups.com/article/view/10.21037/tcr-24-1080/coif). The authors have no conflicts of interest to declare.

Ethical Statement: The authors are accountable for all aspects of the work in ensuring that questions related to the accuracy or integrity of any part of the work are appropriately investigated and resolved. Animal experiments were performed under a project license (No. 2019-153) granted by the Ethics Committee of Gansu University of Chinese Medicine, in compliance with Gansu University of Chinese Medicine guidelines for the care and use of animals.

References

1. Sung H, Ferlay J, Siegel RL, et al. Global Cancer Statistics 2020: GLOBOCAN Estimates of Incidence and Mortality Worldwide for 36 Cancers in 185 Countries. CA Cancer J Clin 2021;71:209-49.
2. Sharma SV, Bell DW, Settleman J, et al. Epidermal growth factor receptor mutations in lung cancer. Nat Rev Cancer 2007;7:169-81.
3. Hirsch FR, Scagliotti GV, Mulshine JL, et al. Lung cancer: current therapies and new targeted treatments. Lancet 2017;389:299-311.
4. Daguenet E, Louati S, Wozny AS, et al. Radiation-induced bystander and abscopal effects: important lessons from preclinical models. Br J Cancer 2020;123:339-48.
5. Prise KM, O'Sullivan JM. Radiation-induced bystander signalling in cancer therapy. Nat Rev Cancer 2009;9:351-60.
6. Havaki S, Kotsinas A, Chronopoulos E, et al. The role of oxidative DNA damage in radiation induced bystander effect. Cancer Lett 2015;356:43-51.
7. Lorimore SA, Coates PJ, Scobie GE, et al. Inflammatory-type responses after exposure to ionizing radiation in vivo:

a mechanism for radiation-induced bystander effects? Oncogene 2001;20:7085-95.
8. Thurairajah K, Broadhead ML, Balogh ZJ. Trauma and Stem Cells: Biology and Potential Therapeutic Implications. Int J Mol Sci 2017;18:577.
9. Hu L, Yin X, Zhang Y, et al. Radiation-induced bystander effects impair transplanted human hematopoietic stem cells via oxidative DNA damage. Blood 2021;137:3339-50.
10. Sémont A, François S, Mouiseddine M, et al. Mesenchymal stem cells increase self-renewal of small intestinal epithelium and accelerate structural recovery after radiation injury. Adv Exp Med Biol 2006;585:19-30.
11. Hang HL, Xia Q. Role of BMSCs in liver regeneration and metastasis after hepatectomy. World J Gastroenterol 2014;20:126-32.
12. Zhang L, Luo Y, Lu Z, et al. Astragalus Polysaccharide Inhibits Ionizing Radiation-Induced Bystander Effects by Regulating MAPK/NF-kB Signaling Pathway in Bone Mesenchymal Stem Cells (BMSCs). Med Sci Monit 2018;24:4649-58.
13. Iyer R, Lehnert BE, Svensson R. Factors underlying the cell growth-related bystander responses to alpha particles. Cancer Res 2000;60:1290-8.
14. Shao C, Folkard M, Prise KM. Role of TGF-beta1 and nitric oxide in the bystander response of irradiated glioma cells. Oncogene 2008;27:434-40.
15. Zhang LY, Yong WX, Wang L, et al. Astragalus Polysaccharide Eases G1 Phase-Correlative Bystander Effects through Mediation of TGF- β R/MAPK/ROS Signal Pathway After Carbon Ion Irradiation in BMSCs. Am J Chin Med 2019;47:595-612.
16. Gong F, Peng X, Luo C, et al. Cathepsin B as a potential prognostic and therapeutic marker for human lung squamous cell carcinoma. Mol Cancer 2013;12:125.
17. Roshy S, Sloane BF, Moin K. Pericellular cathepsin B and malignant progression. Cancer Metastasis Rev 2003;22:271-86.
18. Rozhin J, Sameni M, Ziegler G, et al. Pericellular pH affects distribution and secretion of cathepsin B in malignant cells. Cancer Res 1994;54:6517-25.
19. Shi Q, Shen Q, Liu Y, et al. Increased glucose metabolism in TAMs fuels O-GlcNAcylation of lysosomal Cathepsin B to promote cancer metastasis and chemoresistance. Cancer Cell 2022;40:1207-1222.e10.
20. Zhang X, Wang X, Xu S, et al. Cathepsin B contributes to radioresistance by enhancing homologous recombination in glioblastoma. Biomed Pharmacother 2018;107:390-6.
21. Yuan D, Liu C, Wu J, et al. Inactivation of NSF ATPase Leads to Cathepsin B Release After Transient Cerebral Ischemia. Transl Stroke Res 2018;9:201-13.
22. Man SM, Kanneganti TD. Regulation of lysosomal dynamics and autophagy by CTSB/cathepsin B. Autophagy 2016;12:2504-5.
23. Peng Y, Zhang M, Zheng L, et al. Cysteine protease cathepsin B mediates radiation-induced bystander effects. Nature 2017;547:458-62.
24. Reisenauer A, Eickelberg O, Wille A, et al. Increased carcinogenic potential of myeloid tumor cells induced by aberrant TGF-beta1-signaling and upregulation of cathepsin B. Biol Chem 2007;388:639-50.
25. Adam PJ, Clesham GJ, Flynn PD, et al. Identification and characterisation of transforming growth factor beta-regulated vascular smooth muscle cell genes. Cytokine 2000;12:348-54.
26. Cortés-Ferré HE, Martínez-Avila M, Antunes-Ricardo M, et al. In vitro Evaluation of Anti-Inflammatory Activity of "Habanero" Chili Pepper (Capsicum chinense) Seeds Extracts Pretreated with Cellulase. Plant Foods Hum Nutr 2023;78:109-16.
27. Ullah R, Ikram M, Park TJ, et al. Vanillic Acid, a Bioactive Phenolic Compound, Counteracts LPS-Induced Neurotoxicity by Regulating c-Jun N-Terminal Kinase in Mouse Brain. Int J Mol Sci 2020;22:361.
28. Amin FU, Shah SA, Kim MO. Vanillic acid attenuates Aβ1-42-induced oxidative stress and cognitive impairment in mice. Sci Rep 2017;7:40753.
29. Zhang YM, Zhang LY, Li YY, et al. Radiation-Induced Bystander Effect on the Genome of Bone Marrow Mesenchymal Stem Cells in Lung Cancer. Antioxid Redox Signal 2023;38:747-67.
30. Natewong S, Niwaspragrit C, Ratanachamnong P, et al. Photo-Protective and Anti-Inflammatory Effects of Antidesma thwaitesianum Müll. Arg. Fruit Extract against UVB-Induced Keratinocyte Cell Damage. Molecules 2022;27:5034.
31. Wu C, Sun C, Han X, et al. Sanyin Formula Enhances the Therapeutic Efficacy of Paclitaxel in Triple-Negative Breast Cancer Metastases through the JAK/STAT3 Pathway in Mice. Pharmaceuticals (Basel) 2022;16:9.
32. Piippo N, Korhonen E, Hytti M, et al. Oxidative Stress is the Principal Contributor to Inflammasome Activation in Retinal Pigment Epithelium Cells with Defunct Proteasomes and Autophagy. Cell Physiol Biochem 2018;49:359-67.
33. McKelvey KJ, Hudson AL, Back M, et al. Radiation, inflammation and the immune response in cancer. Mamm

Genome 2018;29:843-65.
34. Grivennikov SI, Greten FR, Karin M. Immunity, inflammation, and cancer. Cell 2010;140:883-99.
35. Barker HE, Paget JT, Khan AA, et al. The tumour microenvironment after radiotherapy: mechanisms of resistance and recurrence. Nat Rev Cancer 2015;15:409-25.
36. Kong FM, Hayman JA, Griffith KA, et al. Final toxicity results of a radiation-dose escalation study in patients with non-small-cell lung cancer (NSCLC): predictors for radiation pneumonitis and fibrosis. Int J Radiat Oncol Biol Phys 2006;65:1075-86.
37. Yang C, Chen XC, Li ZH, et al. SMAD3 promotes autophagy dysregulation by triggering lysosome depletion in tubular epithelial cells in diabetic nephropathy. Autophagy 2021;17:2325-44.
38. Meyer N, Henkel L, Linder B, et al. Autophagy activation, lipotoxicity and lysosomal membrane permeabilization synergize to promote pimozide- and loperamide-induced glioma cell death. Autophagy 2021;17:3424-43.
39. Wei X, Qi Y, Zhang X, et al. ROS act as an upstream signal to mediate cadmium-induced mitophagy in mouse brain. Neurotoxicology 2015;46:19-24.
40. Hou J, Han ZP, Jing YY, et al. Autophagy prevents irradiation injury and maintains stemness through decreasing ROS generation in mesenchymal stem cells. Cell Death Dis 2013;4:e844.
41. Zhang YM, Zhang LY, Zhou H, et al. Astragalus polysaccharide inhibits radiation-induced bystander effects by regulating apoptosis in Bone Mesenchymal Stem Cells (BMSCs). Cell Cycle 2020;19:3195-207.
42. Lamore SD, Wondrak GT. Autophagic-lysosomal dysregulation downstream of cathepsin B inactivation in human skin fibroblasts exposed to UVA. Photochem Photobiol Sci 2012;11:163-72.
43. Zheng L, Wu X, Li S, et al. Cathepsin B inhibitors block multiple radiation-induced side effects in C. elegans. Cell Res 2019;29:1042-5.
44. Bains M, Kaur J, Akhtar A, et al. Anti-inflammatory effects of ellagic acid and vanillic acid against quinolinic acid-induced rat model of Huntington's disease by targeting IKK-NF-κB pathway. Eur J Pharmacol 2022;934:175316.
45. Mei M, Sun H, Xu J, et al. Vanillic acid attenuates H2O2-induced injury in H9c2 cells by regulating mitophagy via the PINK1/Parkin/Mfn2 signaling pathway. Front Pharmacol 2022;13:976156.

Cite this article as: Zhou T, Zhang YM, Zhou GC, Liu FX, Miao ZM, Zhang LY, Li YY, Liu ZW, Zhang SZ, Li J, Niu F, Chen Y, Liu YQ. Vanillic acid inhibits TGF-β type I receptor to protect bone marrow mesenchymal stem cells from radiation-induced bystander effects. Transl Cancer Res 2025;14(2):1223-1236. doi: 10.21037/tcr-24-1080